Vietnam Journal of Mechanics, Vol. 44, No. 4 (2022), pp. 376 – 391
DOI: https://doi.org/10.15625/0866-7136/17911

GEOMETRICALLY NONLINEAR ANALYSIS OF SANDWICH COMPOSITE BEAMS REINFORCED BY AGGLOMERATION CARBON NANOTUBES

Thi Thu Hoai Bui[1,2,*], **Thi Thom Tran**[1,2], **Dinh Kien Nguyen**[1,2]
[1]*Institute of Mechanics, VAST, Hanoi, Vietnam*
[2]*Graduate University of Science and Technology, VAST, Hanoi, Vietnam*
[*]E-mail: thuhoaihus@gmail.com

Received: 01 December 2022 / Published online: 30 December 2022

Abstract. In this work, geometrically nonlinear behavior of sandwich composite beams reinforced by carbon nanotubes is studied, taking into account the influence of agglomeration of the carbon nanotubes (CNTs). The core of the sandwich beams is homogeneous while the two face sheets are made of CNT reinforced composite with the effective material properties being estimated by the Eshelby-Mori-Tanaka approach. A first-order shear deformable nonlinear beam element is formulated in the context of the total Lagrange formulation and used to construct the discretized nonlinear equilibrium equation. The Newton–Raphson based iterative procedure is used in conjunction with the arc-length method to trace the equilibrium paths of the beams. Detail parametric studies are carried out to illustrate the influence of the CNTs agglomeration, the amount of CNT volume fraction as well as the thicknesses of face sheets on the nonlinear behavior of the structure.

Keywords: nanocomposite sandwich beam, agglomeration effect of CNTs, Eshelby-Mori-Tanaka approach, total Lagrange formulation, large deflection analysis.

1. INTRODUCTION

Nonlinear analysis of structures is an important topic in structural mechanics. Since the analytical methods encounter difficulties in dealing with nonlinearities, a numerical method, especially the finite method is often chosen as a replacement. Regarding geometrically nonlinear analysis of beams, the topic discussed herein, several beam elements for the analysis are available in the literature, and some of which have been documented in the textbooks [1,2]. For nonlinear analysis of sandwich beams, Nguyen and Tran [3] performed a large displacement analysis of functionally graded (FG) sandwich beams and frames using a co-rotational Euler–Bernoulli beam element. Hoai et al. [4] derived a nonlinear finite beam element for studying the large displacements of FG sandwich beams,

considering the effect of environment temperature rise. The influence of various homogenization schemes on large deflections of dual-phase FG sandwich beams is investigated by Nguyen et al. [5] using a nonlinear finite element procedure.

Because of the superior mechanical, thermal, electrical, and physical properties, CNTs are outstanding candidate for reinforcing polymer matrix [6, 7]. Investigations on mechanical behavior of carbon nanotubes reinforced composite (CNTRC) sandwich beams have been reported by several authors. However, most of the works have been carried by assuming that the CNTs are aligned in the polymer matrix. The influence of CNTs agglomeration seems to be firstly considered by Kamarian et al. [8] in their free vibration analysis of sandwich beams reinforced by FG-CNTs. The results of the work reveal that the CNTs agglomeration has significant influence on the natural frequencies of the FG-CNTRC sandwich beams. On the basis of the Eringen's nonlocal elasticity theory and the sinusoidal shear deformation theory, Daghigh et al. [9] presented a nonlocal bending and buckling analysis of agglomerated CNTRC nanoplates resting on a Pasternak foundation. They found that the elastic properties of the nanoplates are adversely affected in the presence of CNTs agglomeration and ignoring the agglomeration in numerical modeling of nanocomposites can lead to significant errors.

To the authors' best knowledge, the large deflections of sandwich composite beams reinforced by agglomeration carbon nanotubes have not been reported so far. As an attempt to fill this gap, this paper presents a geometrically nonlinear analysis of CNTRC beams by considering the agglomeration effect of single-wall carbon nanotubes (CNTs). The materials properties of the sandwich composite beams are estimated by the Eshelby–Mori–Tanaka approach. Based on a total Lagrange formulation, a first-order shear deformable nonlinear beam element is formulated and used to construct the nonlinear equilibrium equation for the beams. Newton–Raphson iterative procedure is employed in conjunction with the arc-length method to compute the equilibrium paths of the beams. The influence of CNTs agglomeration, the amount of CNT volume fraction in the face sheets, and the thicknesses of face sheets on the nonlinear behavior of the sandwich beams is examined and discussed.

2. PROBLEM DESCRIPTION

An FGSW beam with length L, rectangular cross section $(b \times h)$ in a Cartesian coordinate system (x, y, z) is shown in Fig. 1. The sandwich beam consists of a homogeneous core and two face sheets made of CNTRC material. The CNTs volume fraction V_{cnt} is assumed to vary in the beam thickness according to

$$V_{cnt}(z) = \begin{cases} V^*_{CNT}\left(1 - \dfrac{z + 0.5}{h_f}\right) \\ 0 \\ V^*_{CNT}\left(1 + \dfrac{z - 0.5}{h_f}\right) \end{cases} \tag{1}$$

where h and h_f are the thickness of the beam and the face sheets, respectively; V^*_{CNT} is the maximum possible amount of CNT volume fraction in the face sheets. According to (1), the core of beam does not contain CNT, whereas the lower and upper face sheets are made of the CNTRC material.

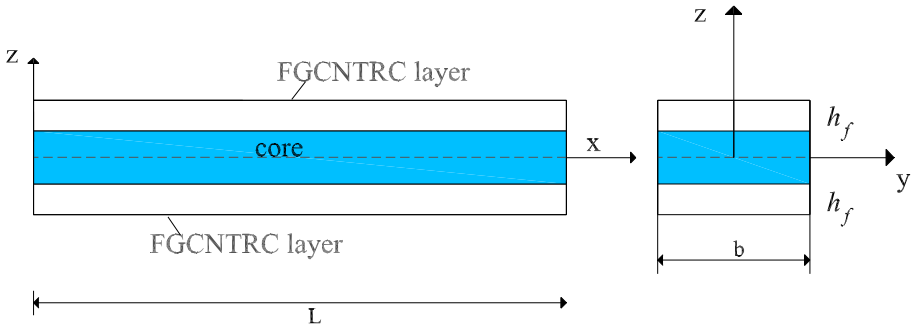

Fig. 1. Geometry of FG-CNTRC sandwich beam

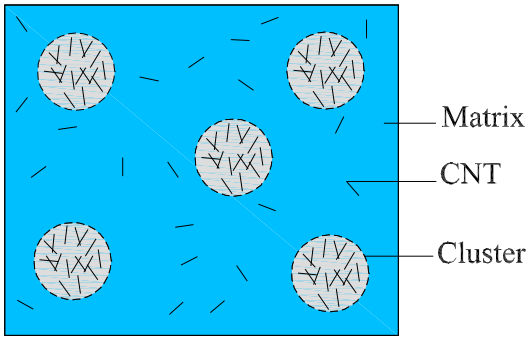

Fig. 2. RVE with Eshelby cluster model of agglomeration of CNTs [8]

It is assumed that a number of CNTs are uniformly distributed (UD) throughout the matrix and the other CNTs appear in cluster form because of agglomeration, as illustrated in Fig. 2. The total volume of CNTs in the representative volume element (RVE), V_r, can be divided into the following two parts

$$V_r = V_r^{cluster} + V_r^m, \tag{2}$$

where $V_r^{cluster}$ represents the volumes of CNTs inside a cluster, and is the volume of CNTs in the matrix and outside the clusters. The two parameters describing the agglomeration are defined as [8]

$$\mu = \frac{V_{cluster}}{V}, \qquad \eta = \frac{V_r^{cluster}}{V_r}, \qquad 0 \leq \eta, \ \mu \leq 1, \tag{3}$$

where V is the volume of RVE, $V_{cluster}$ is the volume of cluster in the RVE. The symbol μ denotes the volume fraction of clusters with respect to the total of the RVE, and η is the

volume ratio of the CNTs inside the clusters over the total CNT inside the RVE. A value of $\mu = 1$ corresponding to the case that all CNTs are uniformly distributed in the matrix, and with the decrease of μ, the agglomeration degree of CNTs is more severe. If $\eta = 1$, all the nanotubes are located in the clusters. The case $\mu = \eta$ means that the volume fraction of CNTs inside the clusters is as same as that of CNTs outside the clusters (fully dispersed). When $\eta > \mu$, the bigger value of η the more heterogeneous the spatial distribution of CNTs. Thus, we consider the CNTRC as a system consisting of clusters of sphere shape embedded in a matrix. First, we may estimate the effective elastic stiffness of cluster and the matrix, respectively; and then calculate the overall property of the whole composite system. The effective bulk modulus K_{in} and shear modulus G_{in} of the cluster and the effective bulk modulus K_{out} and shear modulus G_{out} of the equivalent matrix outside the cluster can be calculated by [8]

$$K_{in} = K_m + \frac{V_{cnt}\eta\left(\delta_r - 3K_m\alpha_r\right)}{3\left(\mu - V_{cnt}\eta + V_{cnt}\eta\alpha_r\right)}, \tag{4}$$

$$K_{out} = K_m + \frac{V_{cnt}\left(1-\eta\right)\left(\delta_r - 3K_m\alpha_r\right)}{3\left[1-\mu - V_{cnt}\left(1-\eta\right) + V_{cnt}\left(1-\eta\right)\alpha_r\right]}, \tag{5}$$

$$G_{in} = G_m + \frac{V_{cnt}\eta\left(\eta_r - 2G_m\beta_r\right)}{2\left(\mu - V_{cnt}\eta + V_{cnt}\eta\beta_r\right)}, \tag{6}$$

$$G_{out} = G_m + \frac{V_{cnt}\left(1-\eta\right)\left(\eta_r - 2G_m\beta_r\right)}{2\left[1-\eta - V_{cnt}\left(1-\eta\right) + V_{cnt}\left(1-\eta\right)\beta_r\right]}, \tag{7}$$

where

$$\alpha_r = \frac{3\left(K_m + G_m\right) + k_r - l_r}{3\left(G_m + k_r\right)}, \tag{8}$$

$$\beta_r = \frac{1}{5}\left\{\frac{4G_m + 2k_r + l_r}{3\left(G_m + k_r\right)} + \frac{4G_m}{G_m + p_r} + \frac{2\left[G_m\left(3K_m + G_m\right) + G_m\left(3K_m + 7G_m\right)\right]}{G_m\left(3K_m + G_m\right) + m_r\left(3K_m + 7G_m\right)}\right\}, \tag{9}$$

$$\delta_r = \frac{1}{3}\left[n_r + 2l_r\frac{\left(2k_r + l_r\right)\left(3K_m + 2G_m - l_r\right)}{G_m + k_r}\right], \tag{10}$$

$$\eta_r = \frac{1}{5}\left[\frac{2}{3}\left(n_r - l_r\right) + \frac{8G_m p_r}{G_m + p_r} + \frac{8m_r G_m\left(3K_m + 4G_m\right)}{3K_m\left(m_r + G_m\right) + G_m\left(7m_r + G_m\right)} + \frac{2\left(k_r - l_r\right)\left(2G_m + l_r\right)}{3\left(G_m + k_r\right)}\right]. \tag{11}$$

The subscripts m and r in the above equations stand for the quantities of the matrix and the reinforcing phase, K_m and G_m are the bulk and shear moduli of the matrix, respectively; k_r, m_r, n_r and p_r are the Hill's elastic moduli for the reinforcing phase (CNTs).

The effective bulk modulus K and the effective shear modulus G of the composite are derived from the Mori–Tanaka method as follows [8]

$$K = K_{out}\left[1 + \frac{\mu\left(\frac{K_{in}}{K_{out}} - 1\right)}{1 + \alpha\left(1-\mu\right)\left(\frac{K_{in}}{K_{out}} - 1\right)}\right], \tag{12}$$

$$G = G_{out}\left[1 + \frac{\mu\left(\frac{G_{in}}{G_{out}} - 1\right)}{1 + \beta\left(1 - \mu\right)\left(\frac{G_{in}}{G_{out}} - 1\right)}\right], \tag{13}$$

in which

$$\nu_{out} = \frac{3K_{out} - 2G_{out}}{2\left(3K_{out} + G_{out}\right)}, \tag{14}$$

$$\alpha = \frac{1 + \nu_{out}}{3\left(1 - \nu_{out}\right)}, \tag{15}$$

$$\beta = \frac{2\left(4 - 5\nu_{out}\right)}{15\left(1 - \nu_{out}\right)}. \tag{16}$$

Finally, the effective Young's modulus E and Poisson's ratio ν of the composite are given by [8]

$$E = \frac{9KG}{3K + G}, \tag{17}$$

$$\nu = \frac{3K - 2G}{6K + 2G}. \tag{18}$$

3. TOTAL LAGRANGE FORMULATION

In this section, a nonlinear finite beam element for large deflection analysis is formulated in the context of the total Lagrange formulation. A two-node shear deformable beam element taking into account the variation of the material properties in the beam thickness is considered herewith. The element with six degrees of freedom, as depicted in Fig. 3, based on the Antman's nonlinear beam model [10] was firstly derived by Pacoste and Eriksson [11] for nonlinear analysis of homogeneous beams. The vector of nodal degrees of freedom is of the form

$$\mathbf{d} = \{u_1 \quad w_1 \quad \theta_1 \quad u_2 \quad w_2 \quad \theta_2\}^T, \tag{19}$$

where u_i, w_i and θ_i $(i = 1, 2)$ are, respectively, the axial, transverse displacements and rotation at node i; the superscript 'T' in Eq. (19) and hereafter, is used to denote the transpose of a vector or a matrix.

The beam element with length l is initially straight and lies on the x-axis as depicted in a Cartesian coordinate system (x, z) in Fig. 3. A point P with abscissa x and its associated cross section S in the initial configuration become point P' and section S' in the deformed configuration. The deformation of the point P can be defined through an angle $\theta(x)$- the rotation of the cross section S, and the current position vector $\mathbf{r}_{,x}\left(x\right)$ of the point P', as [11]

$$\mathbf{r}_{,x}\left(x\right) = \frac{\mathrm{d}\mathbf{r}\left(x\right)}{\mathrm{d}x} = \left[1 + \varepsilon\left(x\right)\right]\mathbf{e}_1 + \gamma\left(x\right)\mathbf{e}_2, \tag{20}$$

where

$$\mathbf{e}_1 = \cos\theta\,\mathbf{i} + \sin\theta\,\mathbf{j}, \qquad \mathbf{e}_2 = -\sin\theta\,\mathbf{i} + \cos\theta\,\mathbf{j}, \tag{21}$$

are the unit vectors, orthogonal and parallel to the current section S', respectively. The curvature of the beam $\kappa(x)$ at the point P' is given by

$$\kappa(x) = \frac{\mathrm{d}\theta(x)}{\mathrm{d}x}. \tag{22}$$

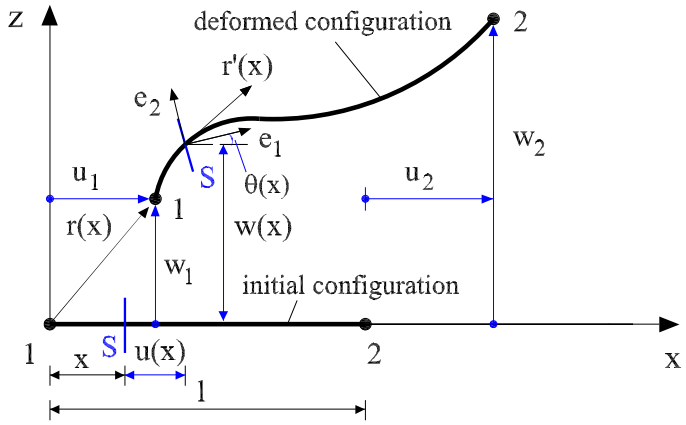

Fig. 3. Configurations and kinematics of a two-node beam element

From Eqs. (20)–(22), one can write the axial and shear strains in the forms

$$\varepsilon(x) = \left(1 + \frac{\mathrm{d}u}{\mathrm{d}x}\right)\cos\theta + \frac{\mathrm{d}w}{\mathrm{d}x}\sin\theta - 1, \quad \gamma(x) = \frac{\mathrm{d}w}{\mathrm{d}x}\cos\theta - \left(1 + \frac{\mathrm{d}u}{\mathrm{d}x}\right)\sin\theta. \tag{23}$$

As emphasized in [11] that the strains $\varepsilon(x), \gamma(x)$ and the curvature $\kappa(x)$ although parameterized for convenience by the reference abscissa $x \in [0, l]$ take the values on the current deformed configuration.

The strain energy for the shear deformable beam element is of the form

$$U = \frac{1}{2}\int_0^l \left[A_{11}\epsilon(x)^2 + 2A_{12}\epsilon(x)\kappa(x) + A_{22}\kappa(x)^2 + \psi A_{33}\gamma(x)^2\right]\mathrm{d}x, \tag{24}$$

where ψ is the shear correction factor, chosen by $5/6$ for the rectangular cross section; A_{11}, A_{12}, A_{22} and A_{33} are, respectively, the axial, axial-bending coupling, bending and shear rigidities, which are defined as

$$\begin{aligned}(A_{11}, A_{12}, A_{22}) &= \int_A E_f^{(k)}(1, z, z^2)\mathrm{d}A = \sum_{k=1}^{3}\int_{z_{k-1}}^{z_k} bE_f^{(k)}(1, z, z^2)\mathrm{d}z,\\ A_{33} &= \int_A G_f^{(k)}\mathrm{d}A = \sum_{k=1}^{3}\int_{z_{k-1}}^{z_k} bG_f^{(k)}\mathrm{d}z,\end{aligned} \tag{25}$$

with A is the cross-sectional area.

The displacements and rotation inside the element of the first-order shear deformation beam element can be linearly interpolated from the nodal values according to

$$u = \frac{l-x}{l}u_1 + \frac{x}{l}u_2\,, \quad w = \frac{l-x}{l}w_1 + \frac{x}{l}w_2\,, \quad \theta = \frac{l-x}{l}\theta_1 + \frac{x}{l}\theta_2. \tag{26}$$

The beam element based on the above linear interpolation functions, however encounters the shear locking problem [4]. In order to overcome this problem, the reduced integration technique, namely one-point Gauss quadrature, is employed herewith to evaluate the strain energy of the element. In this regard, one can express the strain energy in Eq. (24) in the following form

$$U = \frac{l}{2}\left(A_{11}\bar{\varepsilon}^2 + 2A_{12}\bar{\varepsilon}\bar{\kappa} + A_{22}\bar{\kappa}^2 + \psi A_{33}\bar{\gamma}^2\right). \tag{27}$$

In Eq. (27), $\bar{\varepsilon}$, $\bar{\gamma}$ and $\bar{\kappa}$ are given by

$$\begin{cases} \bar{\varepsilon} = \left(1 + \dfrac{u_2 - u_1}{l}\right)\cos\bar{\theta} + \dfrac{w_2 - w_1}{l}\sin\bar{\theta} - 1, \\ \bar{\gamma} = -\left(1 + \dfrac{u_2 - u_1}{l}\right)\sin\bar{\theta} + \dfrac{w_2 - w_1}{l}\cos\bar{\theta}, \\ \bar{\kappa} = \dfrac{\theta_2 - \theta_1}{l}, \end{cases} \tag{28}$$

with

$$\bar{\theta} = \frac{\theta_1 + \theta_2}{2}. \tag{29}$$

The internal force vector $\mathbf{f}_{in}$ for the element is obtained by differentiating the strain energy expression with respect to the nodal displacement vector as

$$\mathbf{f}_{in} = \frac{\partial U}{\partial \mathbf{d}} = \mathbf{f}_a + \mathbf{f}_c + \mathbf{f}_b + \mathbf{f}_s. \tag{30}$$

The element tangent stiffness matrix $\mathbf{k}_t$ is calculated by twice differentiating the strain energy with respect to the nodal displacement vector as follows

$$\mathbf{k}_t = \frac{\partial^2 U}{\partial \mathbf{d}^2} = \mathbf{k}_a + \mathbf{k}_c + \mathbf{k}_b + \mathbf{k}_s. \tag{31}$$

In Eqs. (30)–(31) the subscripts a, c, b, s denote the terms stemming from the axial stretching, axial-bending coupling, bending and shear deformation of the beam, respectively.

Noting that for the nonlinear analysis considered herein, both the internal force vector $\mathbf{f}_{in}$ and the tangent stiffness matrix $\mathbf{k}_t$ depend on the current nodal displacements $\mathbf{d}$. The detailed expressions for the internal force vector in Eq. (30) and the tangent stiffness matrix in Eq. (31) are given by Eqs. (A.1)–(A.6) in the Appendix A.

4. EQUILIBRIUM EQUATION

The equilibrium equation for large deflection analysis of the beam can be written in the form [1]

$$\mathbf{g}(\mathbf{p}, \lambda) = \mathbf{q}_{in}(\mathbf{p}) - \lambda \mathbf{f}_{ex} = \mathbf{0}, \tag{32}$$

where the residual force vector $\mathbf{g}$ is a function of the current structural nodal displacements $\mathbf{p}$ and the load level parameter λ; $\mathbf{q}_{in}$ is the structural nodal force vector, assembled from the formulated vector $\mathbf{f}_{in}$; $\mathbf{f}_{ex}$ is the fixed external loading vector.

The system of Eq. (32) can be solved by an incremental/iterative procedure. The procedure results in a predictor-corrector algorithm, in which a new solution is firstly predicted from a previous converged solution, and then successive corrections are added until a chosen convergence criterion is satisfied. A convergence criterion based on Euclidean norm of the residual force vector is used herein as

$$\|\mathbf{g}\| \leq \epsilon \|\lambda \mathbf{f}_{ex}\|, \tag{33}$$

where ϵ is the tolerance, chosen by 10^{-4} for all numerical examples reported in Section 5.

Newton–Raphson based method is used in combination with the spherical arc-length control technique herein to solve Eq. (32). Detail implementation of the spherical arc-length control method is given in [1].

5. NUMERICAL INVESTIGATION

The numerical results for a nanocomposite CNT-reinforced sandwich beam are presented in this section. Here, we consider PMMA, referred to polymethyl methacrylate, as the matrix which its material properties as follows: $E^m = 2.5\,\text{GPa}$, $v^m = 0.34$. The reinforcement is assumed to be $(10, 10)$ single-walled CNTs (SWCNTs). Otherwise stated, an aspect ratio $L/h = 10$ is chosen for the analysis. The ratio of core thickness to face sheet thickness is defined by h_c/h_f . Representative elastic constants for this CNT are listed in Table 1.

Table 1. Hill's elastic modulus for the CNTs [9]

Bán kính CNT (Å)	k_r (GPa)	l_r (GPa)	m_r (GPa)	n_r (GPa)	p_r (GPa)
10	30	10	1	450	1

The following dimensionless parameters are introduced for the external loads and displacements

$$P^* = \frac{PL^2}{E_m I}, \quad u^* = \frac{u_L}{L}, \quad w^* = \frac{w_L}{L}, \tag{34}$$

where I is the inertia moment of the cross section; E_m is Young's modulus of the polymer matrix; u_L and w_L are the tip axial and transverse displacements, respectively.

To verify the formulation presented in Section 4, the analytical solution for the effective Young's modulus of the CNTRC nanobeam with agglomeration is compared with those of Daghigh et al. [9]. The good agreement result is evaluated based on the available data in Daghigh et al. [9] and shown in Fig. 4. It is worthy to note that the agglomeration has a significant effect on the material properties. The curves in Fig. 4 suggest that having CNTs in a fully-dispersed status results in the highest value of Young's modulus, while the increase of agglomeration degree leads to the decrease of Young's modulus.

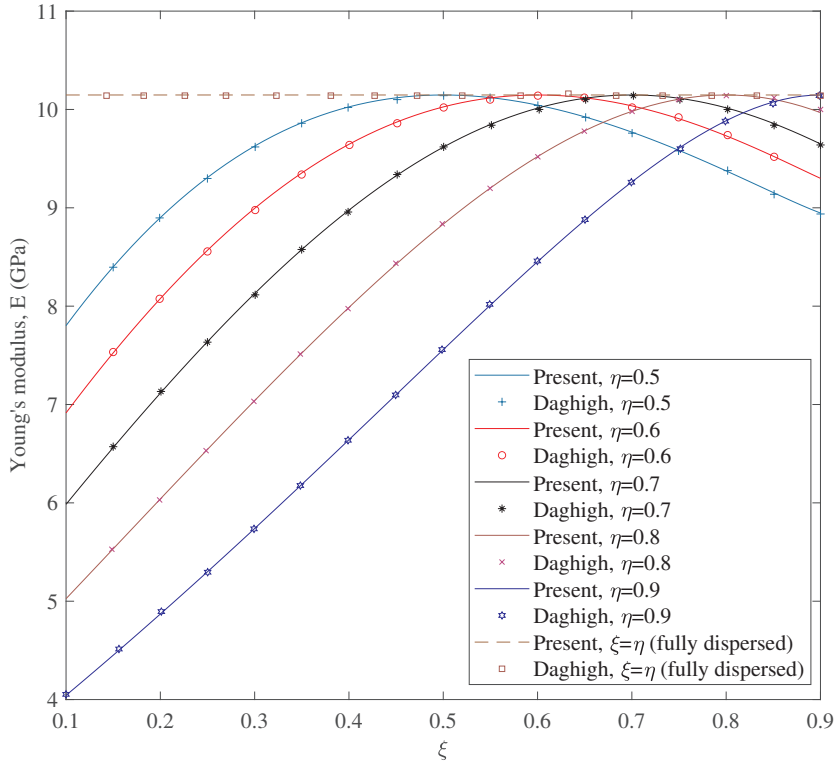

Fig. 4. Effect of CNT agglomeration on the Young's moduli of a CNTRC nanobeam ($V^*_{CNT} = 0.1$)

Next, a cantilever sandwich composite beam reinforced by agglomeration carbon nanotubes under a transverse tip load P is considered. In Figs. 5 and 6, the effect of two parameters used to describe the agglomeration η and μ is depicted for a transverse load $P^* = 15$. The figures confirm that the tip displacement of the sandwich composite beam is larger for the smaller values of the agglomeration parameters. This means that the higher agglomeration is the larger displacement are. Also, one can observed from Figure that with the higher V^*_{CNT} and the smaller value of h_c/h_f, the obtaining load-displacement curves are markedly different.

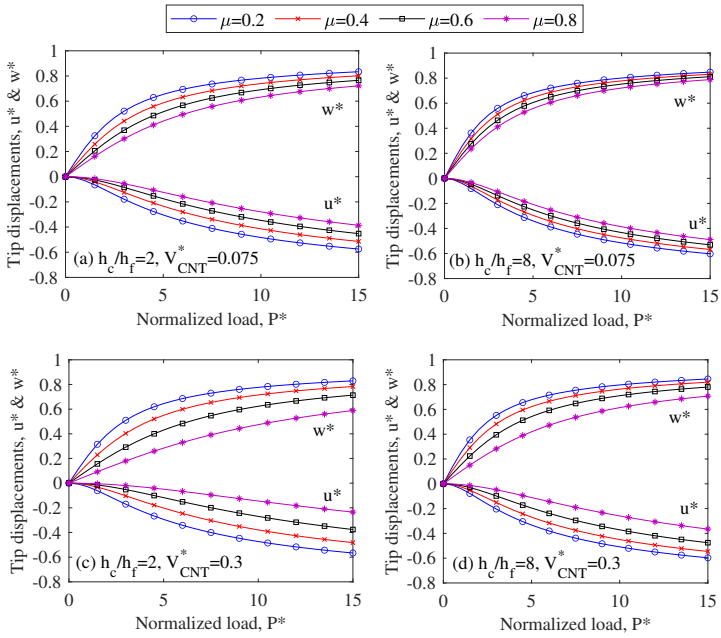

Fig. 5. Effect of agglomeration parameter μ on the load-displacement curves of sandwich composite beam under tip load $(\eta = 1)$

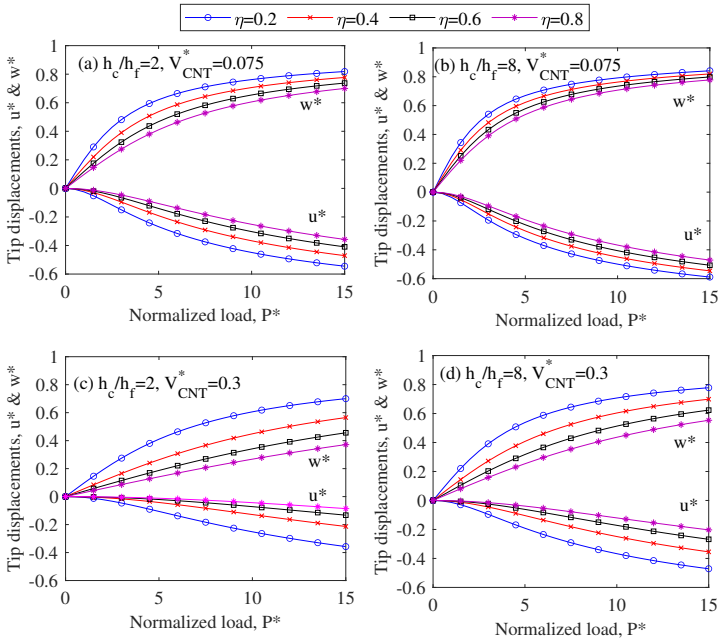

Fig. 6. Effect of agglomeration η parameter on the load-displacement curves of sandwich composite beam under transverse load $(\mu = 1)$

Fig. 7 shows the load-displacement of sandwich composite beam under a tip load $P^* = 15$ at various CNT volume fractions. As can be seen from the figure that an increase in the CNT volume fraction decreases the large displacement response of a sandwich composite beam reinforced by agglomeration carbon nanotubes. The curves corresponding to the higher ratio of core thickness to face sheet thickness (such as $h_c/h_f = 8$ in Fig. 7(d)) get the higher tip displacements compared to that of the smaller ratio of core thickness to face sheet thickness ($h_c/h_f = 2$ in Fig. 7(a)). Fig. 8 confirms again the above remark on the influence of the core-to-face sheet thickness ratio on the large displacement response of the composite beam.

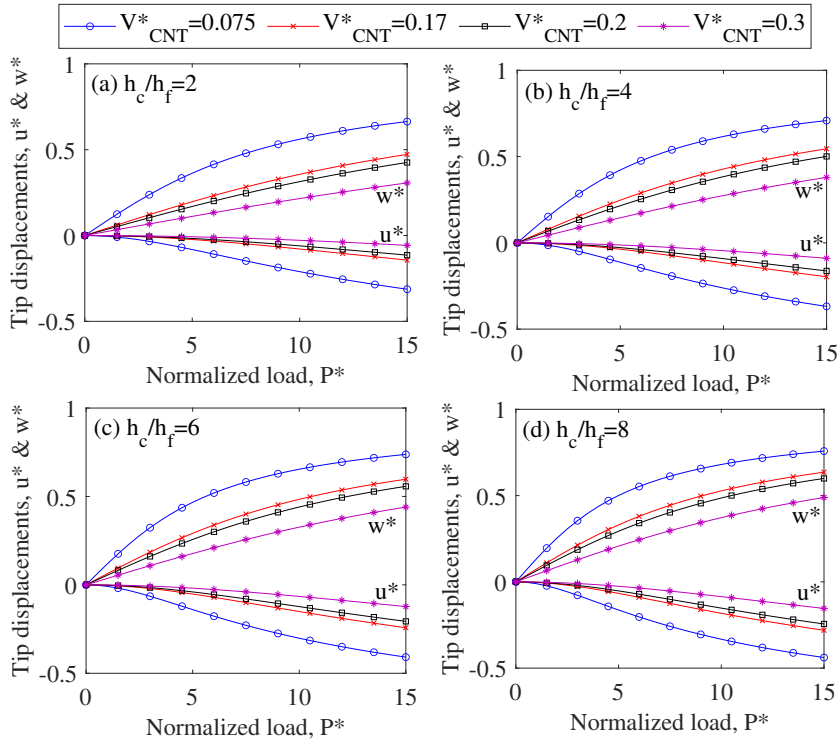

Fig. 7. Effect of V^*_{CNT} on the load-displacement curves of sandwich composite beam under tip load ($\mu = \eta = 0.5$)

The deformed configurations of sandwich composite beam reinforced by agglomeration carbon nanotubes are shown in Fig. 9 for different CNT volume fractions. As mentioned above that having CNT in a fully-dispersed status ($\mu = \eta$) results in the highest value of Young's modulus, the deformed configurations curves from Figs. 9(b) and 9(d) are quite closed to each other, while that corresponding to $\mu = \eta = 0.5$ from Figs. 9(a) and 9(c) are markedly different.

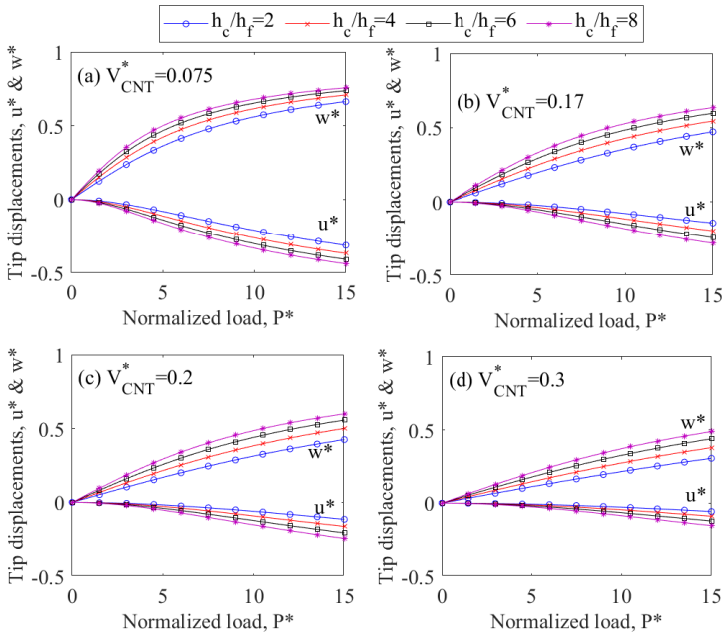

Fig. 8. Effect of h_c/h_f on the load-displacement curves of sandwich composite beam under tip load ($\mu = \eta = 0.5$)

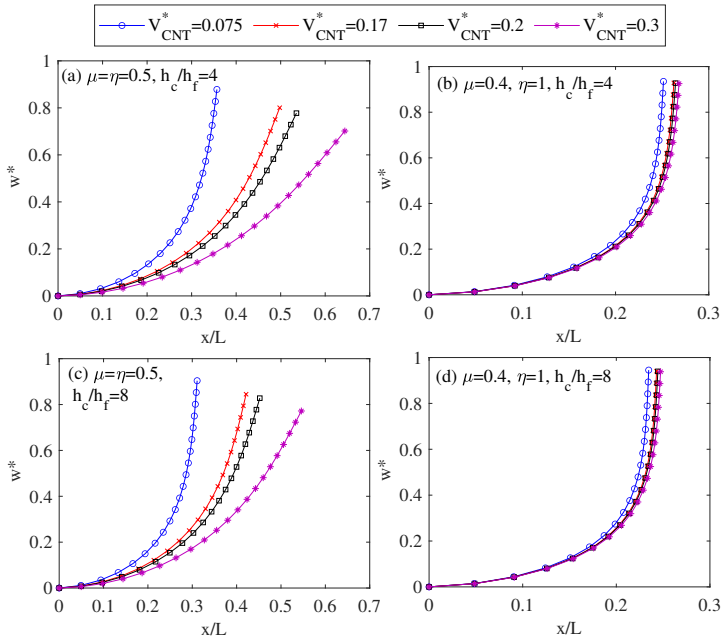

Fig. 9. Deformed configurations of sandwich composite beam corresponding to a transverse tip load $P^* = 50$

6. CONCLUSIONS

The geometrically nonlinear behaviour of sandwich composite beams was investigated by considering the agglomeration effect of single-wall carbon nanotubes using the first-order shear deformable nonlinear beam element and the Mori-Tanaka method. A nonlinear beam element was derived in the context of the total Lagrangian formulation and employed to construct the nonlinear equilibrium equation of the composite beams. Newton-Raphson iterative procedure was used in combination with arc-length method to trace the equilibrium paths of the beams. The numerical investigation reveals that the agglomeration of the CNTs has a significant influence on the nonlinear behaviour of the composite beams, and the nonlinear deflections are larger when the agglomeration degree is more severe. It should be noted that the influence of thermal effect and foundation support, the important factors in behaviour of composite beams in practice, has not considered in the present work. More efforts should be made to take into account the influence of this factors on nonlinear behaviour of agglomerated CNT reinforced composite beams.

DECLARATION OF COMPETING INTEREST

The authors declare that they have no known competing financial interests or personal relationships that could have appeared to influence the work reported in this paper.

ACKNOWLEDGEMENTS

The work presented in this article was supported by the project entitled "Geometrically nonlinear analysis of sandwich composite beams reinforced by agglomeration carbon nanotubes", Institute of Mechanics, and Grant NVCC03.03/22-23, VAST

REFERENCES

[1] M. A. Crisfield. *Non-linear finite element analysis of solids and structures, Volume 1: Essentials*. John Wiley and Sons, Chichester, (1991).

[2] T. Belytschko, W. K. Liu, and B. Moran. *Nonlinear finite elements for continua and structures*. John Wiley & Sons, Chichester, (2000).

[3] D. K. Nguyen and T. T. Tran. A co-rotational formulation for large displacement analysis of functionally graded sandwich beam and frame structures. *Mathematical Problems in Engineering*, (2016), pp. 1–12. https://doi.org/10.1155/2016/5698351.

[4] B. T. T. Hoai, D. K. Nguyen, T. T. T. Huong, and L. T. N. Anh. Large dispalcements of FGSW beams in thermal environment using a finite element formulation. *Vietnam Journal of Mechanics*, **42**, (2020), pp. 43–61. https://doi.org/10.15625/0866-7136/14706.

[5] D. K. Nguyen, T. T. H. Bui, T. T. H. Tran, and S. Alexandrov. Large deflections of functionally graded sandwich beams with influence of homogenization schemes. *Archive of Applied Mechanics*, **92**, (2022), pp. 1757–1775. https://doi.org/10.1007/s00419-022-02140-2.

[6] T. Lau, C. Gu, and D. Hui. A critical review on nanotube and nanotube/nanoclay related polymer composite materials. *Composites Part B: Engineering*, **37**, (2006), pp. 425–436. https://doi.org/10.1016/j.compositesb.2006.02.020.

[7] A. A. Ghorbanpour, S. Maghamikia, and M. Mohammadimehr. Buckling analysis of laminated composite rectangular plates reinforced by SWCNTs using analytical and finite element methods. *Journal of Mechanical Science and Technology*, **25**, (2011), pp. 809–820. https://doi.org/10.1007/s12206-011-0127-3.

[8] S. Kamarian, M. Shakeri, M. H. Yas, M. Bodaghi, and A. Pourasghar. Free vibration analysis of functionally graded nanocomposite sandwich beams resting on Pasternak foundation by considering the agglomeration effect of CNTs. *Journal of Sandwich Structures and Materials*, **17**, (2015), pp. 632–665. https://doi.org/10.1177/1099636215590280.

[9] H. Daghigh, V. Daghigh, A. Milani, D. Tannant, E. L. J. Thomas, and J. N. Reddy. Nonlocal bending and buckling of agglomerated CNT-Reinforced composite nanoplates. *Composites Part B: Engineering*, **183**, (2019). https://doi.org/10.1016/j.compositesb.2019.107716.

[10] S. S. Antman. *Nonlinear problems of elasticity*. Springer-Verlag, New York, (1995). https://doi.org/10.1007/978-1-4757-4147-6.

[11] C. Pacoste and A. Eriksson. Beam elements in instability problems. *Computer Methods in Applied Mechanics and Engineering*, **144**, (1997), pp. 163–197. https://doi.org/10.1016/s0045-7825(96)01165-6.

APPENDIX A.

This Appendix presents detail expressions for the nodal forces and the tangent stiffness matrices in Eq. (30) and Eq. (31). The following notations are used

$$
\begin{aligned}
&s = \sin\bar{\theta}\,, \qquad c = \cos\bar{\theta},\\
&a_1 = (s\bar{\varepsilon} - c\bar{\gamma})\,,\ \ a_2 = (c\bar{\varepsilon} + s\bar{\gamma})\,,\ \ a_3 = \bar{\gamma}^2 - \bar{\varepsilon}\,(1+\bar{\varepsilon})\,,\\
&a_4 = c\bar{\gamma} - s\,(1+\bar{\varepsilon})\,,\ \ a_5 = s\bar{\gamma} + c\,(1+\bar{\varepsilon})\,,\ \ a_6 = (1+\bar{\varepsilon})^2 - \bar{\gamma}^2.
\end{aligned}
\tag{A.1}
$$

The internal force vector

$$
\begin{aligned}
&\mathbf{f}_a = A_{11}\bar{\varepsilon}\left\{-c \ \ -s \ \ \frac{l}{2}\bar{\gamma} \ \ c \ \ s \ \ \frac{l}{2}\bar{\gamma}\right\}^T, \ \ \mathbf{f}_b = A_{22}\bar{\kappa}\{0 \ \ 0 \ \ 1 \ \ 0 \ \ 0 \ \ -1\}^T,\\
&\mathbf{f}_c = A_{12}\bar{\varepsilon}\{0 \ \ 0 \ \ 1 \ \ 0 \ \ 0 \ \ -1\}^T + A_{12}\bar{\kappa}\left\{-c \ \ -s \ \ \frac{l}{2}\bar{\gamma} \ \ c \ \ s \ \ \frac{l}{2}\bar{\gamma}\right\}^T,\\
&\mathbf{f}_s = \psi A_{33}\bar{\gamma}\left\{s \ \ -c \ \ -\frac{l}{2}(1+\bar{\varepsilon}) \ \ -s \ \ c \ \ -\frac{l}{2}(1+\bar{\varepsilon})\right\}^T,
\end{aligned}
\tag{A.2}
$$

$$
\mathbf{k}_a = \frac{1}{l}A_{11}\begin{bmatrix}
c^2 & & & & & \\
sc & s^2 & & sym. & & \\
\frac{l}{2}a_1 & -\frac{l}{2}a_2 & \frac{l^2}{4}a_3 & & & \\
-c^2 & -sc & -\frac{l}{2}a_1 & c^2 & & \\
-sc & -s^2 & \frac{l}{2}a_5 & sc & s^2 & \\
\frac{l}{2}a_1 & -\frac{l}{2}a_2 & \frac{l^2}{4}a_3 & -\frac{l}{2}a_1 & \frac{l}{2}a_2 & \frac{l^2}{4}a_3
\end{bmatrix},
\tag{A.3}
$$

$$
\mathbf{k}_b = \frac{1}{l}A_{22}\begin{bmatrix}
0 & & & & & \\
0 & 0 & & sym. & & \\
0 & 0 & 1 & & & \\
0 & 0 & 0 & 0 & & \\
0 & 0 & 0 & 0 & 0 & \\
0 & 0 & -1 & 0 & 0 & 1
\end{bmatrix},
\tag{A.4}
$$

$$\mathbf{k}_c = A_{12}\bar{\kappa}\begin{bmatrix} 0 & 0 & s & 0 & 0 & s \\ 0 & 0 & -c & 0 & 0 & -c \\ \frac{s}{2} & -\frac{c}{2} & -\frac{l}{2}(1+\bar{\varepsilon}) & -\frac{s}{2} & \frac{c}{2} & \frac{l}{2}(1+\bar{\varepsilon}) \\ 0 & 0 & -s & 0 & 0 & -s \\ 0 & 0 & c & 0 & 0 & c \\ \frac{1}{2}s & -\frac{1}{2}c & -\frac{l}{2}(1+\bar{\varepsilon}) & -\frac{1}{2}s & \frac{1}{2}c & \frac{l}{2}(1+\bar{\varepsilon}) \end{bmatrix} + \frac{2}{l}A_{12}\begin{bmatrix} 0 & 0 & -c & 0 & 0 & c \\ 0 & 0 & -s & 0 & 0 & s \\ 0 & 0 & \frac{l}{2}\bar{\gamma} & 0 & 0 & -\frac{l}{2}\bar{\gamma} \\ 0 & 0 & c & 0 & 0 & -c \\ 0 & 0 & s & 0 & 0 & -s \\ 0 & 0 & \frac{l}{2}\bar{\gamma} & 0 & 0 & -\frac{l}{2}\bar{\gamma} \end{bmatrix}, \tag{A.5}$$

$$\mathbf{k}_s = \frac{\psi}{l}A_{33}\begin{bmatrix} s^2 & & & & & \\ -sc & c^2 & & sym. & & \\ \frac{l}{2}a_4 & \frac{l}{2}a_5 & \frac{l^2}{4}a_6 & & & \\ -s^2 & sc & -\frac{l}{2}a_4 & s^2 & & \\ sc & -c^2 & -\frac{l}{2}a_5 & -sc & c^2 & \\ \frac{l}{2}a_4 & \frac{l}{2}a_5 & \frac{l^2}{4}a_6 & -\frac{l}{2}a_4 & -\frac{l}{2}a_5 & \frac{l^2}{4}a_6 \end{bmatrix}. \tag{A.6}$$